ADAPTIVE ATTITUDE CONTROL OF AN UNMANNED HELICOPTER

Giulia Bertolani[1], Andrea Dan Ryals[2], Fabrizio Giulietti[1] & Lorenzo Pollini[2]

[1]Università di Bologna, Via Fontanelle 40, 47121 Forlì (FC), Italy
[2]Università di Pisa, Via G. Caruso, 16 56122 Pisa(PI), Italy

Abstract

In this paper an $\mathscr{L}_1$ adaptive control system is developed to improve performances and robustness of a baseline Proportional-Integral-Derivative (PID) controller over pitch, roll and yaw axis of a small scale remotely piloted rotorcraft. The proposed control architecture is tested in simulation with a complete non-linear helicopter model. Furthermore, the wind disturbance rejection of the system is investigated. In addition, an on-off switch mechanism is developed in order to disengage adaptive control contribute if needed.

Keywords: L_1 Adaptive, Control, Rotorcraft, Helicopter

1. Introduction

Unmanned Aerial Vehicles (UAV) have become extensively used in a wide range of flight applications, getting a large interest in the scientific and industrial community. In particular, miniature battery-powered fixed and rotary-wings vehicles are suitable for numerous applications, such as load transportation, aerial photography and video shooting, search & rescue, surveillance, tracking etc. Compared to fixed-wing aircrafts, rotorcrafts (multi-rotors and helicopters) have many evident advantages due to their vertical flight and hovering capability [1], [2]. However, these vehicles may operate in potentially obstructed and constrained environments, demanding high capability of the autopilots. For this reason, there is the necessity to design rotorcraft baseline controllers with a considerable high level of robustness against the uncertainties and possible disturbances. The need to improve classical baseline Proportional-Integral-Derivative-based (PID) controllers has contributed to a revived interest in adaptive control techniques, as presented by Anavatti et al. [3].

One promising adaptive control technique is $\mathscr{L}_1$ adaptive control, whose main advantage is to decouple robustness from fast adaptation [4]. As a matter of fact, the use of high adaptation gain induces oscillations in adaptive estimation. To overcome this problem the adaptive input is low-pass filtered. Examples of successful applications in aerospace field are given by Gregory et al. [5], by Wang et al [6] and by Hellmundt et al. [7]. These papers presented utilization almost for fixed-wing aircrafts UAVs. With regards to rotorcrafts, existing literature is mainly related to present simulation results [8], [9], [10], [11]. Tian et al. implemented $\mathscr{L}_1$ control scheme with modified piecewise constant adaptation law [12] for vertical flight control of helicopter. Guerriero et al. used $\mathscr{L}_1$ adaptive control theory to provide attitude and velocity stabilization for an autonomous small-scale helicopter. Bichlmeier et al presented a constant piecewise adaptation law that it is applied on attitude rate control loop. Michini and How tested $\mathscr{L}_1$ on an indoor autonomous quadrotor helicopter. In both the works presented by Tian and Bichlmeier, baseline PID and adaptive control contributions are summed before being passed as input to the system. Moreover, Bichlmeier developed an on-off switching mechanism in order to decide whether using baseline control alone or adding adaptive control contribution.

In this paper an $\mathscr{L}_1$ adaptive control augmentation scheme of a PID linear baseline controller for a small-scale remotely-piloted helicopter is presented. Helicopter dynamics is stabilized trough a PID controller design throughout the flight envelope. PID controller doesn't ensure performances

and robustness which are demanded to $\mathscr{L}_1$ adaptive controller contribution. Adaptive and baseline controllers inputs are summed following the on-off switch structure given by Bichlmeier. The switch structure proves useful during take-off phase and in case of lack of responsiveness to control inputs that may lead to bad adaptation laws behaviour. Implemented $\mathscr{L}_1$ adaptive control structure follows the one presented in [13] for nonlinear systems.

A nonlinear model of a small-scale remotely piloted helicopter has been used to test the proposed control laws. The classic main and tail rotor configuration is considered. Simulations are carried out in Matlab/Simulink® environment,that is used to implement the vehicle model and control laws. The FlightGear® environment serves for visualization purposes.

The paper is organized as follows: section 2. presents the $\mathscr{L}_1$ adaptive control theory; section 3. introduces the helicopter model used for simulations; in section 4. the baseline and $\mathscr{L}_1$ adaptive control systems architectures are described; in section 5. simulations results are given; finally a section 6.of concluding marks ends this paper.

2. $\mathscr{L}_1$ adaptive control
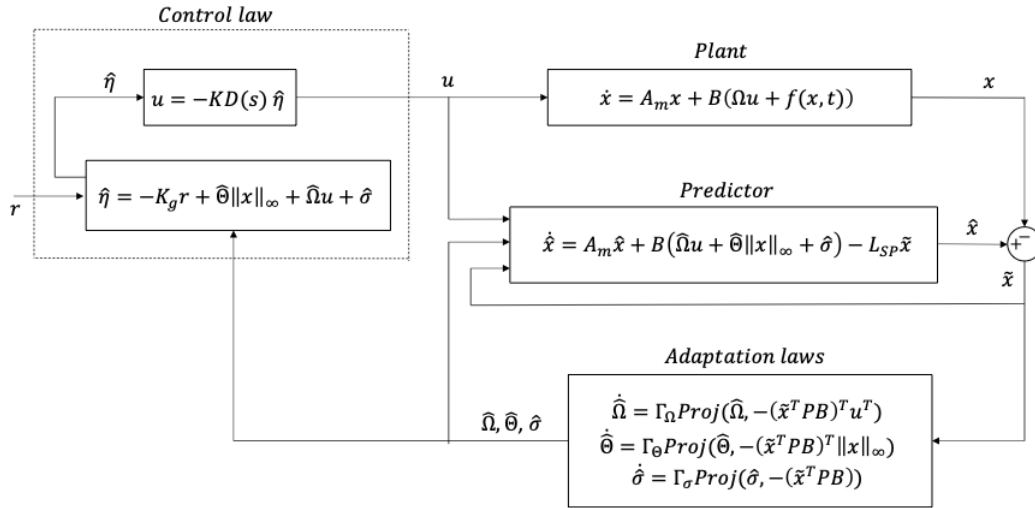
Figure 1 – $\mathscr{L}_1$ adaptive control scheme.

Let the system dynamics be described by the following equations:

$$\dot{x}(t) = A_m x(t) + B_m(\Omega u(t) + f(x(t),t)), x(0) = x_0$$
$$y(t) = Cx(t)$$

(1)

where $x(t) \in \mathbb{R}^n$ is the measured system state, $A_m \in \mathbb{R}^{n \times n}$ is a known Hurwitz matrix specifyng the desired closed loop dynamics; $B \in \mathbb{R}^{n \times m}$ and $C \in \mathbb{R}^{r \times n}$ are known constant matrix, $u(t) \in \mathbb{R}^m$ is the control input; $\Omega \in \mathbb{R}^{m \times m}$ is an unknown constant matrix with diagonal terms of known signs, representing the uncertainty in the system input gain; $f(t,x) : \mathbb{R} \times \mathbb{R}^n \to \mathbb{R}^m$ is an unknown nonlinear map continuous in its arguments which represents system nonlinear uncertainties; $y(t) \in \mathbb{R}^n$ is the regulated output. The initial condition x_0 is assumed to be inside an arbitrarily large known set $||x_0||_\infty \leq \rho_0$. It is assumed that the nonlinear uncertainties map satisfies the semiglobal lipschiz condition for all $||x||_\infty \leq \delta$ and $||\bar{x}||_\infty \leq \delta$, such that

$$|f(x,t) - f(\bar{x},t)| \leq L||x - \bar{x}||_\infty$$

(2a)

$$|f(0,t)| \leq B$$

(2b)

The control objective is to design a state feedback adaptive controller to ensure that $y(t)$ tracks a given reference signal $r(t)$.

2.1 State predictor

State predictor consists of the following equations:

$$\dot{\hat{x}}(t) = A_m\hat{x}(t) + B_m(\hat{\Omega}u(t) + \hat{\Theta}(t)\|x(t)\|_\infty + \hat{\sigma}(t)) - L_{sp}\tilde{x}(t), \hat{x}(0) = \hat{x}_0,$$
$$\hat{y}(t) = C\hat{x}(t), \tag{3}$$

where $\hat{\Omega} \in \mathbb{R}^{m \times m}$, $\hat{\Theta} \in \mathbb{R}^m$, $\hat{\sigma} \in \mathbb{R}^m$ are adaptive estimates obtained as results of $\mathscr{L}_1$ controller adaptation laws. L_{sp} is a positive definite diagonal matrix used to assign faster poles to the prediction error dynamics and $\tilde{x}(t) = \hat{x}(t) - x(t)$ i the error dynamics. It is assumed that system uncertainties $f(x,t)$ could be parameterized as $\hat{f}(x,t) = \hat{\Theta}(t)\|x(t)\|_\infty + \hat{\sigma}(t)$.

2.2 Adaptation Laws

The adaptation laws for $\hat{\Omega}$, $\hat{\Theta}$ and $\hat{\sigma}$ are defined as:

$$\dot{\hat{\Omega}}(t) = \Gamma_\Omega Proj(\hat{\Omega}(t), -(\tilde{x}^T(t)PB)^T u^T(t)), \hat{\Omega}(0) = \hat{\Omega}_0,$$
$$\dot{\hat{\Theta}}(t) = \Gamma_\Theta Proj(\hat{\Theta}(t), -(\tilde{x}^T(t)PB)^T\|x(t)\|_\infty), \hat{\Theta}(0) = \hat{\Theta}_0, \tag{4}$$
$$\dot{\hat{\sigma}}(t) = \Gamma_\sigma Proj(\hat{\sigma}(t), -\tilde{x}^T(t)PB), \hat{\sigma}(0) = \hat{\sigma}_0$$

where $\tilde{x}(t) = \hat{x}(t) - x(t)$ is the prediction error, $\Gamma_\Omega, \Gamma_\Theta, \Gamma_\sigma \in \mathbb{R}^{n \times n}$ are the adaptation gains, $P = P^T > 0$ is the solution to the Lyapunov equation $A_m^T P + A_m P = -Q$ for arbitrary $Q = Q^T > 0$ and the $Proj(.,.)$ denotes the projection operator as defined in [14]. The projection operator ensures that $\hat{\Omega}(t) \in \Omega_s$, $\|\hat{\Theta}_i(t)\|_\infty \le \Theta_b$ and $\|\hat{\sigma}_i(t)\|_\infty \le \sigma_b$, where Ω_s is a compact convex set which includes estimated input gain matrix and Θ_b, σ_b are adaptation terms bounds.

2.3 Control law

The control signal is generated as the output of the following feedback system:

$$u(s) = -KD(s)\hat{\eta}(s), \tag{5}$$

where $K \in \mathbb{R}^{m \times m}$ is a diagonal feedback gain matrix, $D(s)$ is a strictly proper transfer function and $\hat{\eta}(t)$ is the Laplace transform of the following expression:

$$\hat{\eta}(t) = \hat{\Omega}u(t) + \hat{\Theta}(t)\|x(t)\|_\infty + \hat{\sigma}(t) - K_g r(t) \tag{6}$$

where $K_g = -(C^T A_m^{-1}B)^{-1}$ and $r(t)$ is the reference signal. Let's choose $D(s) = \frac{1}{s}\mathbb{I}_m$, where $\mathbb{I}_m$ is the identity matrix of size m. Assuming that the adaptive estimation of the uncertainty input gain $\hat{\Omega}$ converges to Ω after a transient time, the input $u(s)$ to the system in equations (1) and the predictor in equations (3) is filtered trough

$$C(s) = \Omega K(s\mathbb{I}_m + \Omega K)^{-1} \tag{7}$$

where $C(s)$ is a strictly proper filter with DC gain $C(0) = \mathbb{I}_m$. K and $D(s)$ need to ensure that exists a positive ρ_r such that:

$$\|G(s)\|_{\mathscr{L}_1} < \frac{\rho_r - \|K_g C(s)H(s)\|_{\mathscr{L}_1}\|r\|_\infty - \|\rho_0\|_{\mathscr{L}_1}}{L_\rho \rho_r + B} \tag{8}$$

where

$$H(s) = (s\mathbb{I}_n - A_m)^{-1}B, \tag{9a}$$
$$G(s) = H(s)(\mathbb{I}_m - C(s)), \tag{9b}$$
$$\rho_0 = (s\mathbb{I}_n - A_m)^{-1}x_0 \tag{9c}$$

and $L_\rho = \Theta_b$, $B = \sigma_b$. As stated in [13], the upper bound in equation (8) is a consequence of equation (2). If $f(x,t)$ is globally Lipschitz with uniform Lipschitz constant L, then $\rho_r \to \infty$ and the upper bound in equation (8) degenerates into

$$\|G(s)\|_{\mathscr{L}_1} < \frac{1}{L_\rho} \tag{10}$$

3. Helicopter model

A classical conventional configuration is considered, i.e. with one main rotor and one tail rotor. The helicopter is modelled as a rigid body. Resultant forces and moments are the sum of the contributions of the gravitational forces and of the helicopter components, i.e. main rotor, tail rotor and fuselage. These are applied to the vehicle center of mass. The following assumptions are made:

1. The Earth is flat and not-rotating;

2. Mass and mass distribution are assumed to be constants and the aircrtaft is symmetrical with respecet to the X-Z plane.

3. Earth gravity field is uniform;

Let $\mathbb{F}_E = \{O; \mathbf{x}_E, \mathbf{y}_E, \mathbf{z}_E\}$ be the North-Est-Down (NED) frame; $\mathbb{F}_{hw} = \{H; \mathbf{x}_{hw}, \mathbf{y}_{hw}, \mathbf{z}_{hw}\}$ be the Hub-Wind frame, whose origin is in the helicopter hub; $\mathbb{F}_{hb} = \{H; \mathbf{x}_{hb}, \mathbf{y}_{hb}, \mathbf{z}_{hb}\}$ the Hub-Body frame, that conincides with the Hub-Wind when the system sideslip is zero, and $\mathbb{F}_b = \{P; \mathbf{x}_b, \mathbf{y}_b, \mathbf{z}_b\}$ the Body frame, located at the helicopter center of gravity.

Helicopter dynamics is described by Newton-Euler equations of motion projected in the body system of reference $\mathbb{F}_b$. Namely:

$$\dot{\mathbf{V}} = -\boldsymbol{\Omega} \times \mathbf{V} + \mathbf{F}^{(e)}/m \tag{11}$$

$$\dot{\boldsymbol{\Omega}} = \mathbf{I}^{-1}[-\boldsymbol{\Omega} \times (\mathbf{I}\boldsymbol{\Omega}) + \mathbf{M}^{(e)}] \tag{12}$$

where mass and mass distribution are assumed to be constant. $\mathbf{V}$ is the body velocity vector; $\boldsymbol{\Omega}$ is the body angular rate vector; $\mathbf{F}^{(e)}$ and $\mathbf{M}^{(e)}$ are respectively the external forces and moments vectors, $\mathbf{I}$ is the inertial matrix. The external forces are made of aerodynamic forces $\mathbf{F}^{(a)}$ and gravity forces $\mathbf{F}^{(g)}$ contributions, whereas total moments include aerodynamic moments $\mathbf{M}^{(a)}$. Gravity forces are expressed in the following way:

$$\mathbf{F}^{(g)} = \Pi_{be} \begin{bmatrix} 0 \\ 0 \\ mg \end{bmatrix} = \begin{bmatrix} -mg\sin\theta \\ mg\sin\phi\cos\theta \\ mg\cos\phi\cos\psi \end{bmatrix} \tag{13}$$

Aerodynamic effects are introduced for all rotorcraft components and summed:

$$\mathbf{F}^{(a)} = \mathbf{F}^{(main\ rotor)} + \mathbf{F}^{(fuselage)} + \mathbf{F}^{(tail\ rotor)} \tag{14}$$

$$\mathbf{M}^{(a)} = \mathbf{M}^{(main\ rotor)} + \mathbf{M}^{(fuselage)} + \mathbf{M}^{(tail\ rotor)} \tag{15}$$

3.1 Main rotor model

Main rotor is the primary source of lift, propulsion and control, thus it dominates the helicopter dynamics behaviour. Equations are derived for a counter-clockwise rotor and then, by means of symmetrical coordinate systems [15], equations for the clockwise rotor are obtained. The hinge-less rotor is modelled as a teetering one, but the equivalent rotor stiffness K_β is introduced as a correction of the ideal teetering model. Blades are assumed rigid with integral form dependent on control actions, vehicle kinematics and flapping equations. Flapping dynamic is approximated using a tip-path plane representation [16]. The following assumptions are introduced:

1. Rotor blade is rigid in bending and torsion;

2. Linear blade twist;

3. Flapping and inflow angles are assumed small, the analysis is based on a simple strip theory;

4. Only effects due to angular acceleration $\dot{p}$ and $\dot{q}$, angular velocity p, q and the normal acceleration of the aircraft motion are considered to calculate blade flapping;

5. Compressibility and stall effects are not considered;

6. Reversed flow region is not considered;

7. The inflow is assumed to be uniform;

8. The tip loss factor is assumed to be 1;

9. Blade flapping is approximated by the first harmonic terms with time-varying coefficients, that is:

$$\beta(t) = a_0(t) - a_1(t)\cos\psi - b_1(t)\sin\psi \tag{16}$$

The analytical tip-path plane dynamic equations are:

$$\ddot{\mathbf{a}} + \tilde{D}\dot{\mathbf{a}} + \tilde{K}\mathbf{a} = \tilde{\bar{\mathbf{f}}} \tag{17}$$

where $\mathbf{a} = \begin{pmatrix} a_0 & a_1 & b_1 \end{pmatrix}^T$ and expressions for $\tilde{D}$, $\tilde{K}$ and $\tilde{f}$ are reported in [16]. a_0, a_1 and b_1 are respectively the blade coning angle, the longitudinal and lateral flapping angles. According to blade flapping approximation in Eq. (16), a_0, is treated as a preset constant and coefficients $a_1(t)$ and $b_1(t)$ can be solved for by setting $\varepsilon = \dot{a}_0 = \ddot{a}_0$ in equation (17). Given the above assumptions, momentum theory is utilized and blade forces are analytically integrated over the radius. Detailed expressions for the derivation of forces and moments are given in Ref. [16]. Concerning the inflow modelling, the Pitt-Peters dynamic inflow model [17] has been used, only considering a uniform inflow.

3.2 Tail rotor model and Fuselage

The tail rotor is modelled as in [16], in which flapping dynamic is ignored. Thus, flapping angles and forces and moments are obtained as steady state solution. The inflow is uniform and it is a steady state solution of the Pitt-Peters model [17]. It is solved through a Newton-Ralphson iterative method. The fuselage is represented as a virtual flat plate drag source having three dimensions [18]. Forces and moments are evaluated as functions of the angle of attack and of the sideslip angle.

4. Control system architecture

In the proposed control architecture, both PID and $\mathscr{L}_1$ adaptive controller run in parallel and control inputs contributions are summed. $\mathscr{L}_1$ adaptive controller may be switched on or off as needed. Controlled states are roll angle ϕ, pitch angle θ and yaw rate r. This states are normalized to assume values in the closed interval $[-1,1]$. This is achieved by dividing roll and pitch angles by the factor $rad_{max} = 0.7854\ rad$ and the yaw rate by $yawrate_{max} = 1.5\ \frac{rad}{s}$. Inputs computed by controllers belongs to the same interval $[-1,1]$.

4.1 Baseline controller

The baseline loop consists of a PID controller allowing for attitude stabilization and for heading hold. It is organized as a cascade control system [19], in which a primary controller and a primary dynamics are components of the outer loop. A secondary control loop is designed as part of the outer loop, since this primary control loop calculates the set point for the secondary one. Hence the name "cascade control". Moreover, the inner loop should represent a significantly faster dynamics related to the outer loop. This assumption allows to restrain interactions that can occur between them and improve stability characteristics. Thus, a higher gain in the inner loop can be set. Angular rates and attitudes are used as measured feedback signals.
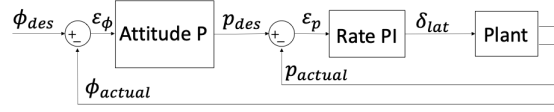
(a) *Roll controller architecture.*
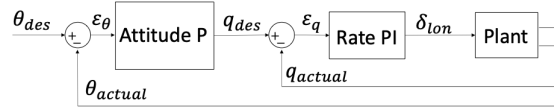
(b) *Pitch controller architecture.*

Figure 2 – Attitude controller architecture.

4.1.1 Attitude controller

Figures 2 shows the controller architecture for attitude control.

The outer loop deals with the Euler angles ϕ and θ, respectively, the roll and the pitch angles. It utilizes attitude estimations calculated into the helicopter model during the simulations. Here a proportional gain is used. The inner loop concerns with the angular velocities in a PI scheme. Let's define the following error signals:

$$\begin{cases} \varepsilon_\phi = \phi_{des} - \phi \\ \varepsilon_\theta = \theta_{des} - \theta \\ \varepsilon_p = p_{des} - p \\ \varepsilon_q = q_{des} - q \end{cases} \tag{18}$$

The cascade P-PI control output can be written as follows:

$$\begin{cases} p_{des} = K_{P\phi}\varepsilon_\phi \\ q_{des} = K_{P\theta}\varepsilon_\theta \\ \delta_{lat} = K_{Pp}\varepsilon_p + K_{Ip}\int_0^t \varepsilon_p dt \\ \delta_{lon} = K_{Pq}\varepsilon_q + K_{Iq}\int_0^t \varepsilon_q dt \end{cases} \tag{19}$$

where K_P are the proportional gains and K_I the integral gains, referred to the proper variables.

4.1.2 Heading hold controller

Figure 3 shows the design of the heading hold controller.

This architecture is similar to that presented for attitude controller, the only difference appears in dealing the user's input signal. As a matter of fact, it provides direct control on the yaw rate r instead of on the real heading angle ψ. The ψ_{des} reference for the outer loop is obtained integrating the ε_r signal, starting from an appropriate initial value. By defining the error signals as follows:

$$\begin{cases} \varepsilon_\psi = \int_0^t \varepsilon_r dt \\ \varepsilon_r = r_{des} - r \end{cases} \tag{20}$$

6
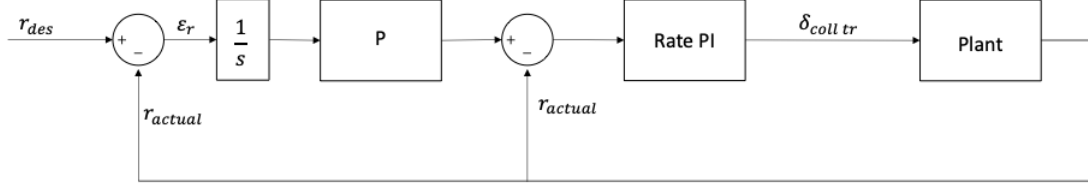
Figure 3 – Example of a figure.

The cascade P-PI control output results to be:

$$\begin{cases} r_{des} = K_{P\psi}\varepsilon_\psi \\ \delta_{coll\ tr} = K_{Pr}\varepsilon_r + K_{Ir}\int_0^t \varepsilon_r dt \end{cases} \tag{21}$$

4.2 $\mathscr{L}_1$ adaptive controller

In this application an $\mathscr{L}_1$ adaptive controller is designed to increase performances of PID baseline control system.

4.2.1 Reference dynamics

The reference dynamics adopted in the predictor, that $\mathscr{L}_1$ controller has to track, are the following:

$$\phi(s) = \frac{6}{s+6}\delta_{lat}(s) \tag{22a}$$

$$\theta(s) = \frac{6}{s+6}\delta_{lon}(s) \tag{22b}$$

$$r(s) = \frac{4}{s+4}\delta_{coll\ tr}(s) \tag{22c}$$

where ϕ, θ and r are roll angle, pitch angle and yaw rate respectively. δ_{lat}, δ_{lon} and $\delta_{coll\ tr}$ are the lateral cyclic, longitudinal cyclic and tail rotor collective control inputs. Reference dynamics are stable and uncoupled, letting the adaptive system to adapt and reduce coupling effects. Given closed loop desired model as in equations (22), reference matrices are $A_m = -diag(6,6,4)$, $B = diag(6,6,4)$ and $C = \mathbb{I}_m$.

4.2.2 Low pass filter shaping

Assuming that $f(x,t)$ is globally Lipschitz, $C(s)$ is shaped such that condition in equation (10) is always satisfied. This is achieved by choosing the right feedback gain matrix K and the set Ω_s. Selected K results as follows

$$K = \begin{bmatrix} 30 & 0 & 0 \\ 0 & 30 & 0 \\ 0 & 0 & 1 \end{bmatrix} \tag{23}$$

Since Ω has to be strictly diagonally dominant, one possible Ω_s that satisfy also this condition is

$$\Omega_s = \begin{bmatrix} [0.75, 1.25] & [-0.35, 0.35] & [-0.35, 0.35] \\ [-0.35, 0.35] & [0.75, 1.25] & [-0.35, 0.35] \\ [-0.35, 0.35] & [-0.35, 0.35] & [0.75, 1.25] \end{bmatrix} \tag{24}$$

Using this Ω_s and the K matrix of equation (23), considering that adaptation estimates limits are $|\Theta_b| = 1$, $|\sigma_b| = 1$, and so $L_\rho = 1$, $B = 1$, condition given in equation (10) is always satisfied.

4.2.3 Estimation laws and predictor shaping

$\mathscr{L}_1$ adaptive control decouples estimation from control. The adaptation laws gains $\Gamma_\Omega, \Gamma_\Theta, \Gamma_\sigma$ should have the greater possible values in order to achieve the fastest possible estimation. However there are limitations that come from the hardware on which the $\mathscr{L}_1$ adaptive control runs on. Satisfactory adaptation gains values are selected by a trial and error procedure during simulations. Control systems sample time is set $T_s = 0.004$. Final chosen values are $\Gamma_\Omega = \Gamma_\Theta = \Gamma_\sigma = \Gamma = diag\,(5000, 5000, 3000)$. $Q = \mathbb{I}_n$ is chosen in order to solve the Lyapunov equation needed to compute P matrix in equations (4). Error dynamics is shaped trough L_{sp} matrix. Satisfactory results are obtained by the following values $L_{sp} = diag(60, 60, 240)$.

4.3 Baseline augmentation

$\mathscr{L}_1$ adaptive control is designed to work in parallel with the baseline PID controllers. Figure (4) shows the selected architecture highlighting the $\mathscr{L}_1$ switch. Inputs computed by baseline and $\mathscr{L}_1$ controllers are summed together, but the switch may be used to cut off adaptive control contribution. This design choice has two main reasons. On one hand, there is the necessity to test the helicopter actuators on ground. In this condition, a lack of response of the helicopter to a pilot command could bring to a wrong estimation of the $\mathscr{L}_1$ adaptive terms. This could contribute to destabilize the helicopter and force the saturation of the actuators before flying. Thus, take off maneuver is performed with $\mathscr{L}_1$ controller switched-off. On the other hand, it is possible to perform safe flight tests through the use of a secure $\mathscr{L}_1$ switch in case of malfunctioning.
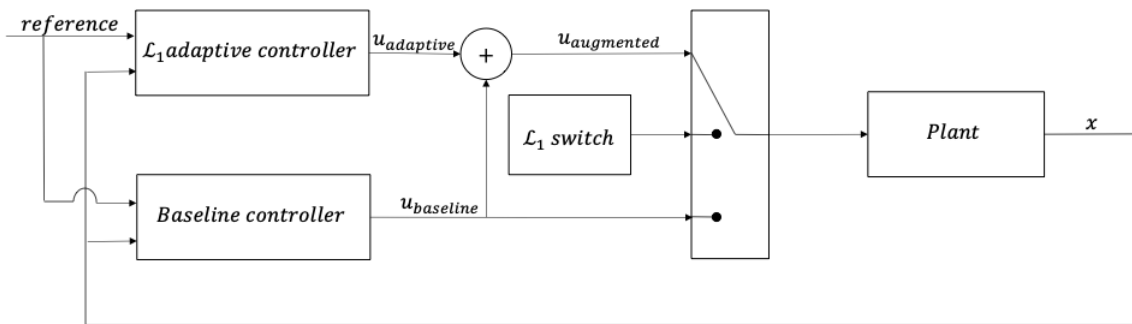
Figure 4 – $\mathscr{L}_1$ augmentation of baseline PID.

5. Simulation results

In this section, simulation results are presented. The full nonlinear dynamic model presented in 3. is here used, parameterized for the remotely-piloted SAB® Goblin700 Thunder helicopter, whose main

parameters are reported in table 1. Simulations are ran in Matlab/Simulink® environment. With the aim to evaluate handling qualities, the FlightGear® flight simulator is used for visualisation purposes, as in Figure 5.

Table 1 – Relevant helicopter data

Parameter	Symbol	Value	Units
Vehicle data			
Mass	m	4.8	kg
Principal moments of inertia	I_x, I_y, I_z	0.0465, 0.2971, 0.2567	kg m^2
Inertia products	I_{xy}, I_{yz}, I_{xz}	0.0079, 0.0033, 0.0006	kg m^2
Stationline position of CG	STA_{CG}	0.34	m
Buttline position of CG.	BL_{CG}	0	m
Waterline position of CG.	WL_{CG}	0.174	m
Main rotor data			
Stationline position of hub	STA_H	0.3305	m
Buttline position of hub	BL_H	0	m
Waterline position of hub	WL_H	0.35	m
Number of rotor blades	N_{blades}	2	
Nominal angular velocity	Ω_{nom}	1995.3	RPM
Radius	R	0.79	m
Mean blade chord	$\bar{c}$	0.06	m
Flapping spring constant	K_β	162.69	Nm/rad
Pitch-flap coupling tangent of δ_3	K_1	0	
Virtual hinge offset	ε	0.0314	m
Blade Inertia moment	I_β	0.0344	kg m^2
Blade profile lift curve slope	$C_{l\alpha}$	2π	rad^{-1}
Blade twist angle	θ_{tw}	0	rad
Precone angle (required for teetering rotor)	a_0	0	rad
Solidity	σ	0.0479	
Shaft tilt	$\frac{\Gamma}{2}$	0.0524	rad
Tail rotor data			
Stationline position of hub	STA_H	1.385	m
Buttline position of hub	BL_H	0.052	m
Waterline position of hub	WL_H	0.205	m
Number of rotor blades	N_{blades}	2	
Nominal angular velocity	Ω_{nom}	9976	RPM
Radius	R	0.115	m
Mean blade chord	$\bar{c}$	0.031	m
Solidity	σ	0.1716	
Pitch-flap coupling tangent of δ_3	K_1	0	
Blade Inertia moment	I_β	0.00002665	kg m^2
Blade profile lift curve slope	$C_{l\alpha}$	2π	rad^{-1}
Blade twist angle	θ_{tw}	0	rad
Fuselage			
Stationline position of fuselage	STA_H	0	m
Buttline position of fuselage	BL_H	0	m
Waterline position of fuselage	WL_H	0	m
Frontal area	S_{front}	0.02042	m^2
Lateral area	S_{front}	0.0633	m^2
Top area	S_{front}	0.09739	m^2
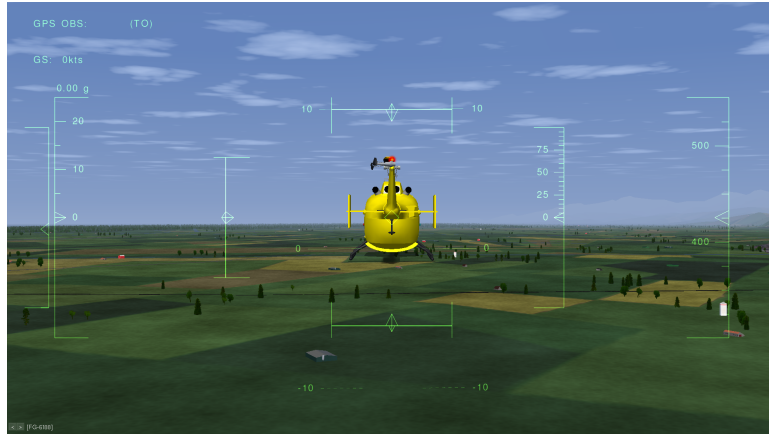
Figure 5 – FlightGear flight simulator

5.1 Baseline vs Augmented control

The first simulation result presented is a comparison between baseline and augmented control. The helicopter follows a simple sequence of two steps as reference signal starting from the hovering trim condition. In figure 6a pitch response to a first step input of $2.5\ deg$ at $20\ s$ of simulation and to a second step of $-10\ deg$ at $70\ s$ is reported. The baseline controller has a slower response to step inputs compared to the augmented system. This is also confirmed by figure 6b, where roll is asked to track a first step input of $5\ deg$ at $20\ s$ and a second step of $-5\ deg$ at $70\ s$. Finally, yawrate response to a first step input of $5\ \frac{deg}{s}$ at time $20\ s$ and to a second step of $-5\ \frac{deg}{s}$ at time $70\ s$ is showed in figure 6c. For all the axes, the augmented controller is able to improve the system performances, especially in operational regions far from the baseline design point. Similar results are presented in figures 7a, 7b 7c. Herein, pitch angle, roll angle and yawrate responses to different step inputs are reported. Again, the initial condition is set to an equilibrium one, that is the hovering.

In figure 8 a simulated test flight is illustrated. In this test the helicopter is piloted trough a joystick by an human operator through the use of the FlightGear® interface. Pilot control commands are recorded and used both to test baseline performances and augmented control performances. As expected, augmented control systems performances lead to smaller errors achieving desired helicopter response. Couplings effects are also mitigated. In figure 9 the three axis normalized inputs are showed. $\mathscr{L}_1$ adaptive control contributes is only a fraction of the control signal as it appears by comparing baseline and augmented control simulations inputs. Figures 10a, 10b, 10c and 10d show adaptation parameters during the same flight.

5.2 $\mathscr{L}_1$ switch

$\mathscr{L}_1$ on/off switch procedure effects on pitch angle, roll angle and yawrate is illustrated in figures 11a, 11b, 11c. A zero value of the switch signal means that $\mathscr{L}_1$ control is off, while a value of 1 means that $\mathscr{L}_1$ control is on. The switching procedure is performed in simulation while helicopter is in hovering, that is a trim condition. As soon as the $\mathscr{L}_1$ controller is switched on, pitch angle, roll angle and yawrate set to reference values after a small spike. The switching off procedure is less critical, unless on the yaw axis, for which the procedure induces a spike that do not affect the flight.

5.3 Wind disturbance rejection

Wind disturbance rejection towards three mathematical representations of wind is tested in this work. The first type is the wind shear model, whose implementation is based on the mathematical theory in the Military Specification MIL-F-8785C [20]. Wind speed at $6\ m$ of altitude is set to $15\ m/s$ with a direction of $0\ degrees$ clockwise from north. The second wind disturbance is a discrete wind gust on all the three axes, that starts at $5\ s$ with a gust amplitude of $[u_g v_g w_g] = [3.5\ 3.5\ 3.0]\ m/s$, where u_g, v_g and w_g are the gust components. The third disturbance is the discrete Dryden wind turbulence model, that uses the Dryden spectral representation to add the turbulence as in reference [21]. Wind speed at $6\ m$ is set to $15\ m/s$ with a direction of $0\ degrees$ clockwise from north. Results are showed
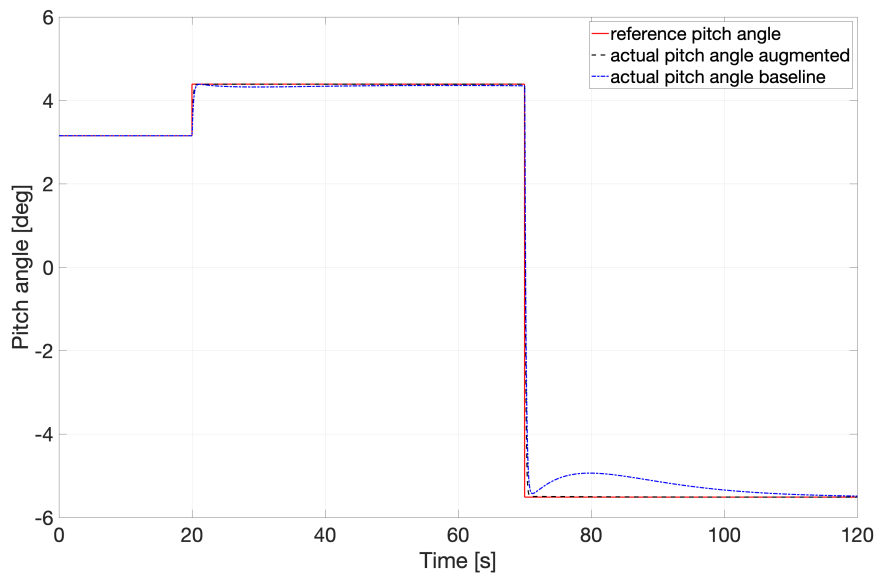
(a) Pitch reference tracking, baseline PID vs augmented PID.
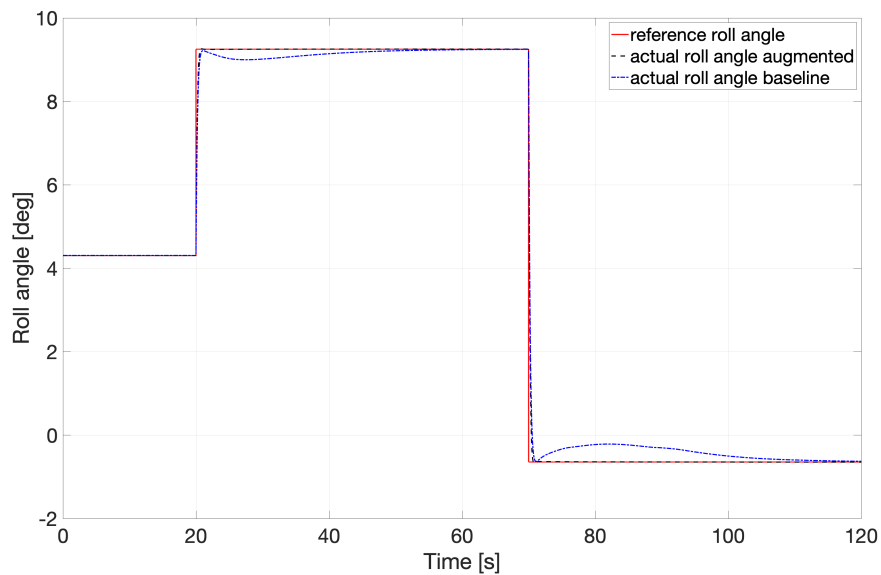
(b) Roll reference tracking, baseline PID vs augmented PID.
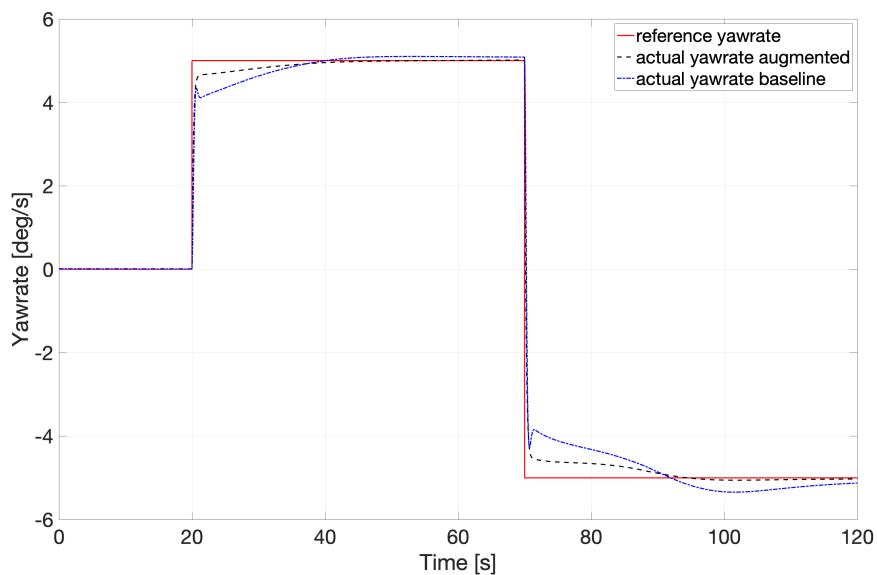
(c) Yawrate reference tracking baseline PID vs augmented PID.

Figure 6 – Reference tracking baseline PID vs augmented PID.
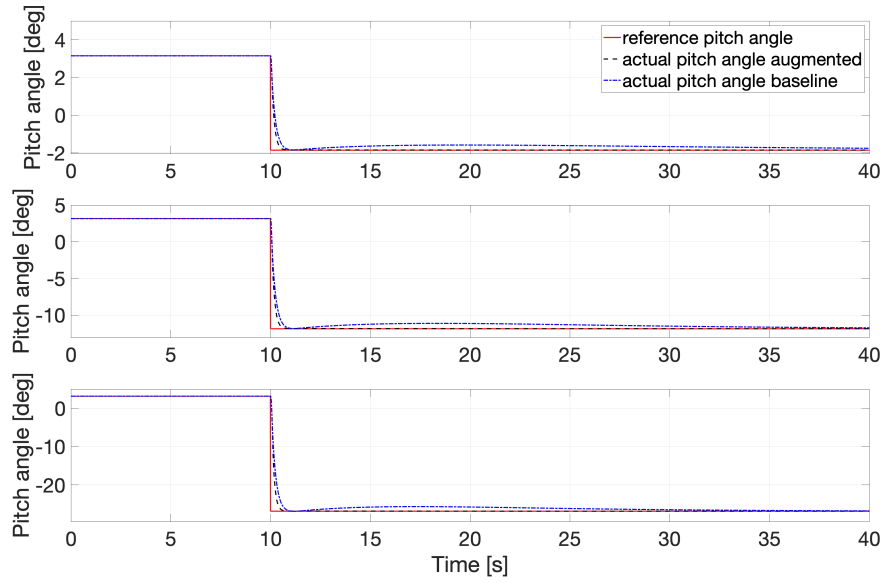
(a) Multiple pitch reference tracking, baseline PID vs augmented PID.
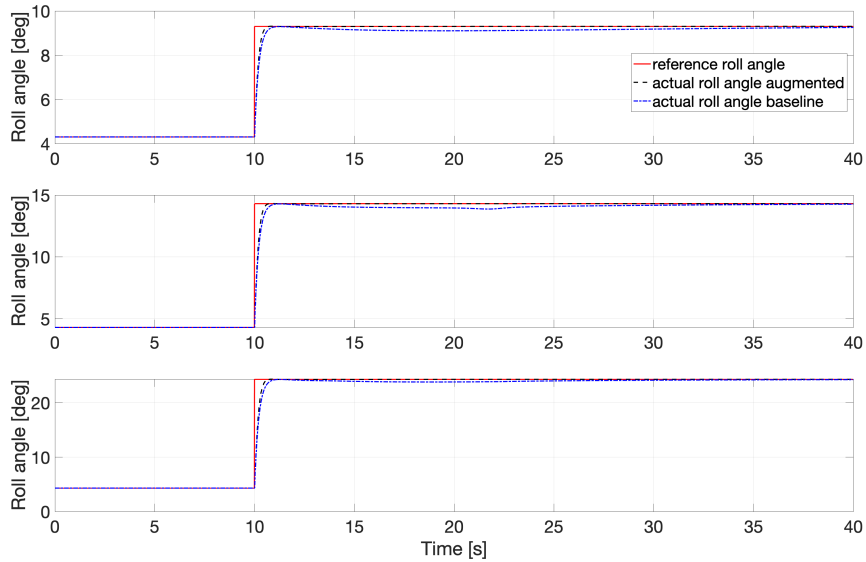
(b) Multiple roll reference tracking, baseline PID vs augmented PID.
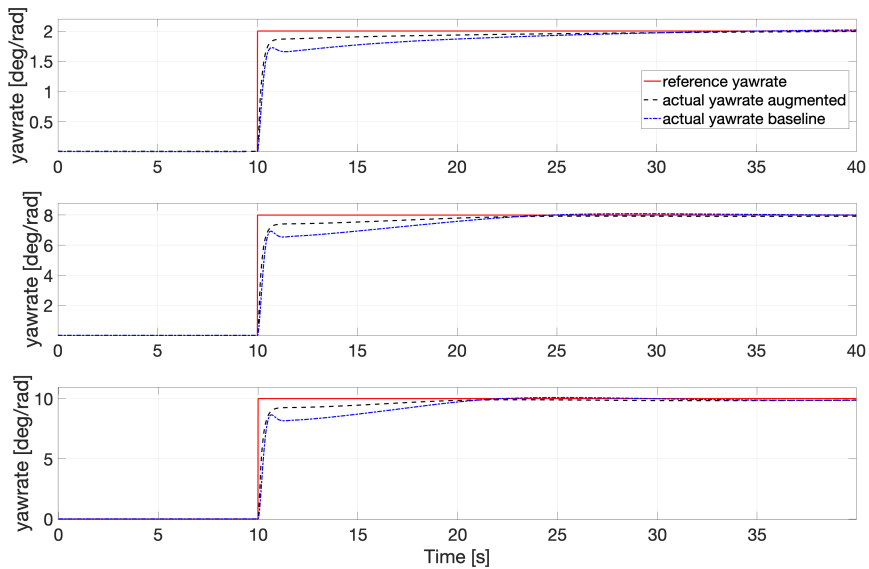
(c) Multiple yawrate reference tracking, baseline PID vs augmented PID.

Figure 7 – Multiple Reference tracking baseline PID vs augmented PID.
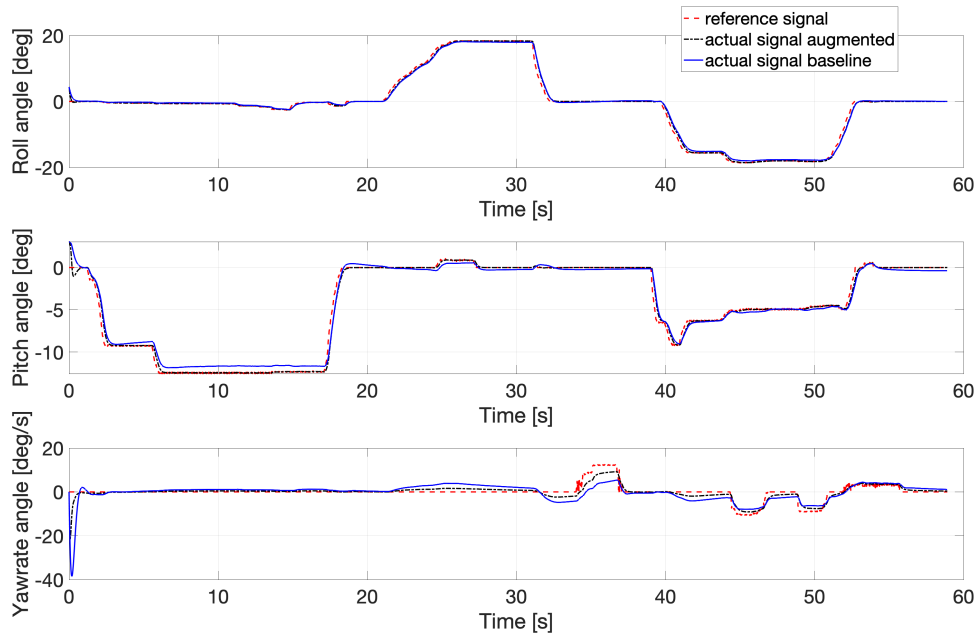
Figure 8 – Attitude and yawrate in simulation.

in figure 12, in which all the presented wind models are combined together. The simulated flight is the same presented in figure 8, aside from the inclusion of the three wind models. The augmented controller presents better reference tracking capabilities even in presence of wind disturbance with respect to the baseline controller.

6. Conclusions

An augmented controller made of a PID baseline controller for system stabilization and an $\mathcal{L}_1$ adaptive controller, was developed and numerically tested for dealing with nonlinear uncertainties and disturbances in a small-scale helicopter application. The two controllers run in parallel and the adaptive component can be safely switched on/ off without showing undesired behaviours. The augmented control system allows the helicopter to improve attitude reference tracking performances and to follow the desired dynamics. Disturbance rejection is investigated trough the combination of three wind models. Simulations show that the performances are improved also in this condition and that the augmented system avoids to lose helicopter attitude control. Despite the behaviour on lateral and longitudinal axes are satisfactory, on the yaw axis there is still the need to improve the augmented controller behaviour. Current design leads to noisy adaptation terms estimation in some flight conditions, especially on the yaw axis. This could be caused both from a poor tuning of the baseline controller and from the need to improve the reference dynamics. For future work, a refinement of the PID baseline tuning will be done. Accordingly, the reference dynamics will be revised. Flight tests on a small scale remotely piloted helicopter platform are scheduled.

7. Contact Author Email Address

giulia.bertolani2@unibo.it
andrea.ryals@phd.unipi.it
fabrizio.giulietti@unibo.it
lorenzo.pollini@unipi.it

8. Copyright Statement
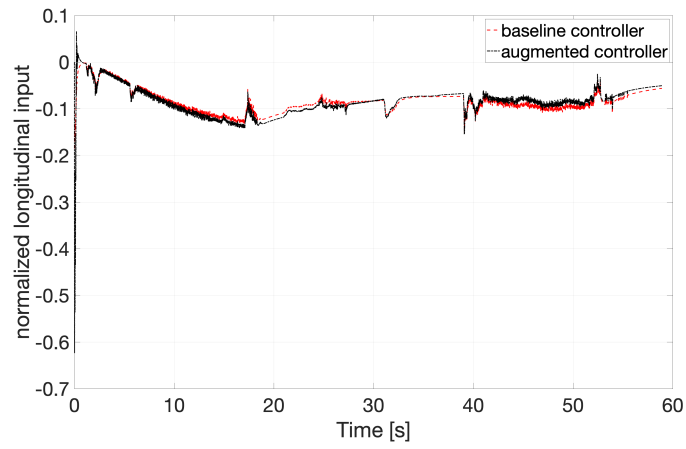
(a) Normalized longitudinal input.
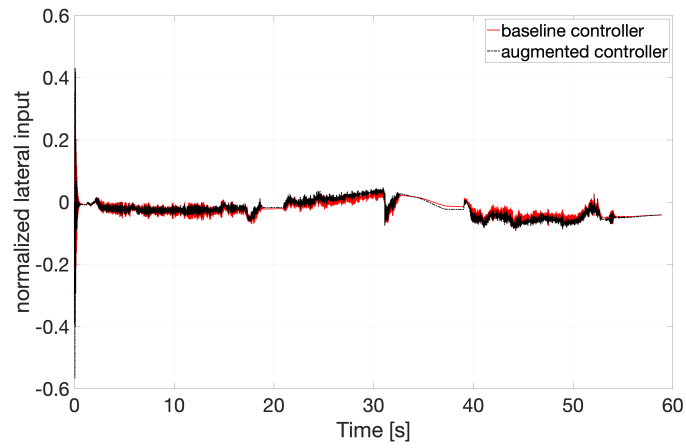
(b) Normalized lateral input.
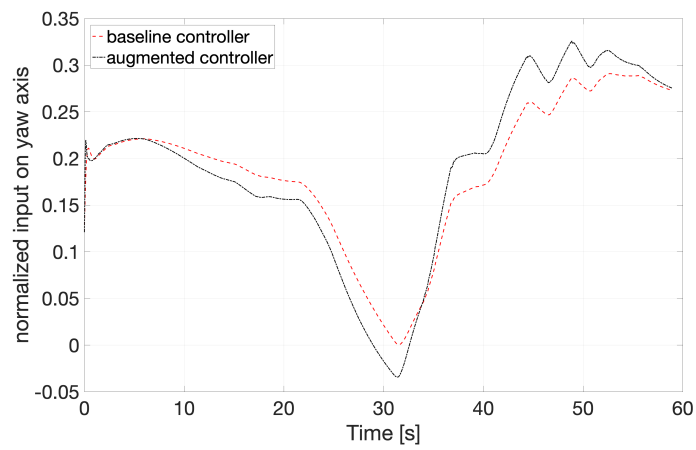
(c) Normalized yaw input.

Figure 9 – Helicopter normalized inputs.
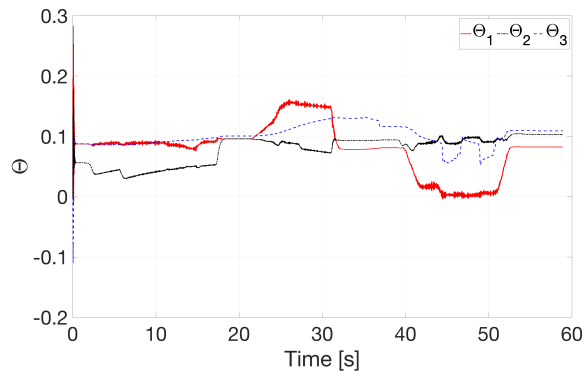
(a) Theta.
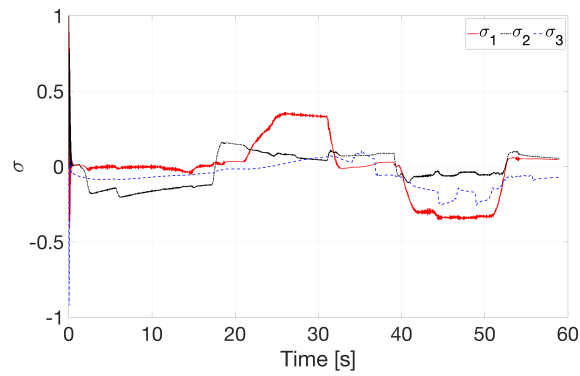
(b) Sigma
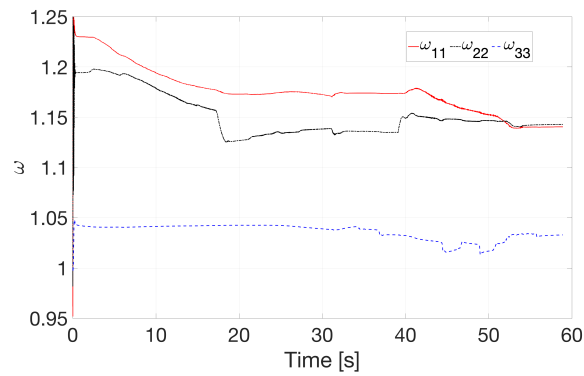
(c) Omega diagonal terms.
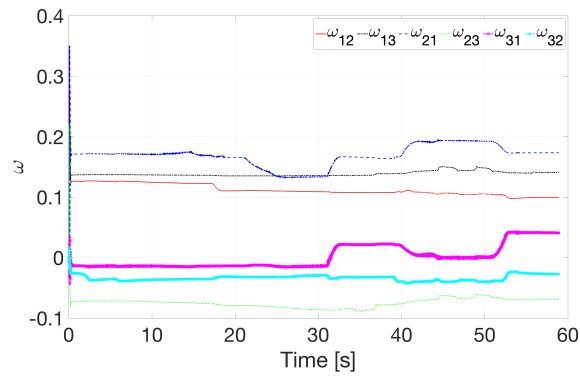
(d) Omega extra-diagonal terms.

Figure 10 – Adaptation terms over time.
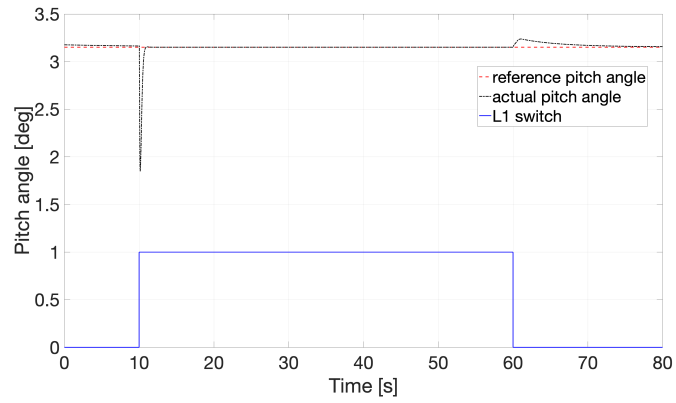
(a) Switch effect on pitch.
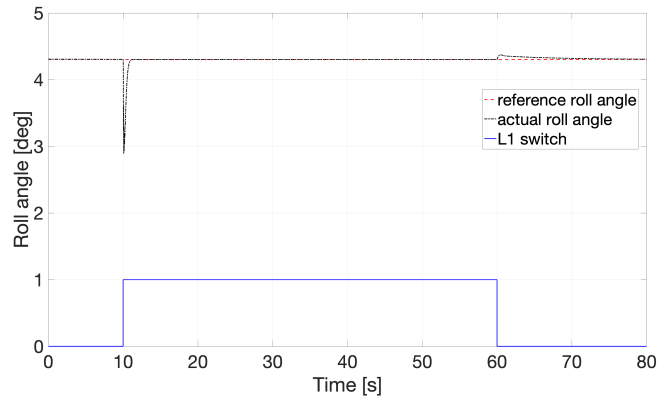
(b) Switch effect on roll.
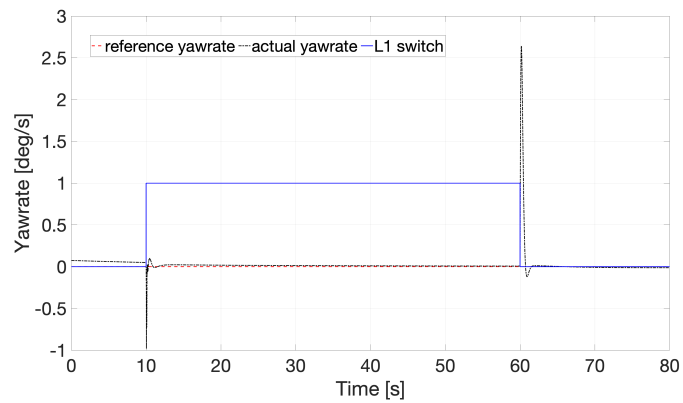
(c) Switch effect on yawrate.

Figure 11 – Switch effect on attitude and yawrate.
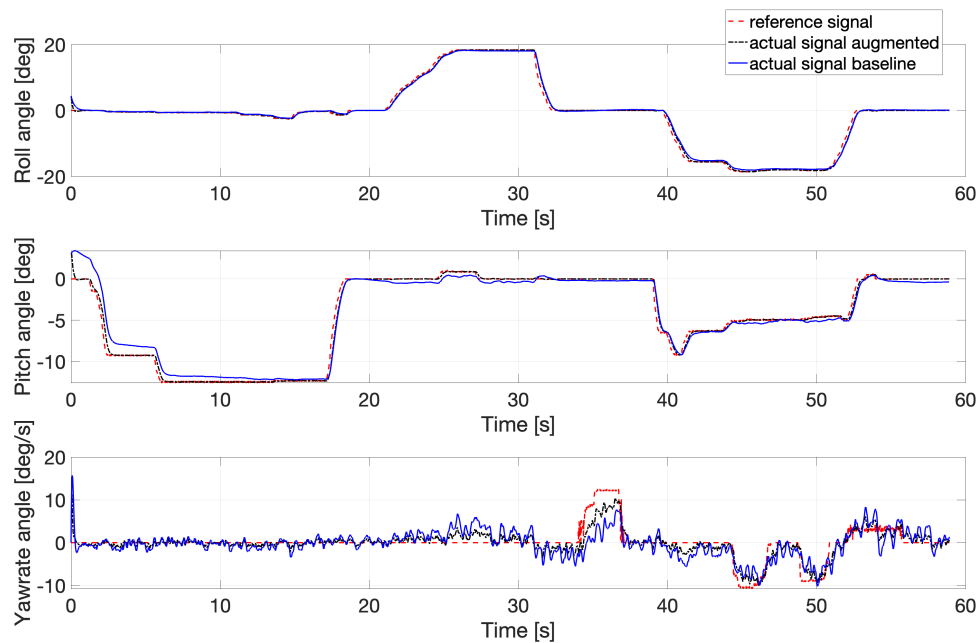
Figure 12 – Combined model wind rejection.

References

[1] Kumar V, Michael N. Opportunities and challenges with autonomous micro aerial vehicles. *The International Journal of Robotics Research*, Vol.31, No. 11, pp 1279–1291, 2012.

[2] Cai G, Dias J, Seneviratne L. A survey of small-scale unmanned aerial vehicles: recent advances and future development trends. *Unmanned Systems*, Vol. 2, No. 2, pp. 175-199, 2014.

[3] Anavatti S G, Santoso F, Garratt M A. Progress in adaptive control systems: past, present, and future. International Conference on Advanced Mechatronics, Intelligent Manufacture, and Industrial Automation (ICAMIMIA), pp. 1-8, 2015.

[4] Hovakimyan N, Cao C. *L1 adaptive control theory: guaranteed robustness with fast adaptation*. Society for Industrial and Applied Mathematics, USA, 2010.

[5] Gregory I, Cao C, Xargay E, Hovakimyan N, Zou X. L1 adaptive control design for NASA AirSTAR flight test vehicle. AIAA Guidance, Navigation, and Control Conference, Chicago, IL. 2009.

[6] Wang J, Vijay V P, Cao C, Hovakimyan N, Lavretsky E. Novel L1 adaptive control methodology for aerial refueling with guaranteed transient performance. *Journal of Guidance Control and Dynamics*, Vol. 31, pp. 182-193, 2008.

[7] Hellmundt F, Wildschek A, Maier R, Osterhuber R, Holzapfel F Comparison of L1 Adaptive Augmentation Strategies for a Differential PI Baseline Controller on a Longitudinal F16 Aircraft Model, *Advances in Aerospace Guidance, Navigation and Control*, pp. 99-118, 2018.

[8] Song T, Wang J, Lin D, Pei P. L1 adaptive control design of a helicopter in vertical flight.*Proceedings of the Institution of Mechanical Engineers, Part G: Journal of Aerospace Engineering*, Vol. 234, No. 14, pp. 2089–99, 2020.

[9] Guerreiro B J, Silvestre C, Cunha R, Cao C, Hovakimyan N. L1 adaptive control for autonomous rotorcraft, American Control Conference, pp. 3250-3255, 2009.

[10] Bichlmeier M, Holzapfel F, Xargay E, Hovakimyan N. L1 adaptive augmentation of a helicopter baseline controller. AIAA Guidance, Navigation, and Control (GNC) Conference, 2013.

[11] Michini B, How J. L1 adaptive control for indoor autonomous vehicles: design process and flight testing. AIAA Guidance, Navigation, and Control Conference, 10 - 13 August, Chicago, Illinois, 2009.

[12] Chengyu C, Hovakimyan N. L1 adaptive output-feedback controller for non-strictly-positive-real reference systems: missile longitudinal autopilot design. *Journal of guidance, control, and dynamics*, Vol. 32, No. 3, pp. 717-726, 2009.

[13] Cao C, Hovakimyan N. L1 adaptive controller for a class of systems with unknown nonlinearities. American Control Conference, pp. 4093-4098, 2008.

[14] Lavretsky E, Gibson T. Projection operator in adaptive systems. arXiv e-Prints, 2011.

[15] Choi H S, Kim E T, You D I, Shim H. Improvements in small-scale helicopter rotor modeling for the real-time simulation of hovering flight, *The Japan Society for Aeronautical and Space Science*, Vol.54, No.185/186, pp.229-37, 2011.

[16] Talbot P D, Tinling B E, Decker W A, Chen R T N. A mathematical model for a single main rotor helicopter for piloted simulation, Ames Reasearch Center, Mffett, Field, California, Sept. 1982.

[17] Peters D A, HaQuang N. Dynamic inflow for practical applications, *Journal of the American Helicopter Society*, Vol.33, No.4 pp.64-68, 1988.

[18] Heffley R K, Mnich M A. Minimum-complexity helicopter simulation math model, Ames Reasearch Center, Mffett, Field, California, Apr. 1988.

[19] Szafranski G, Roman C. Different approaches of PID control UAV type quadrotor. The international micro air vehicles conference. pp. 70-75, 2011.

[20] U.S. Military Specification MIL-F-8785C, November 5, 1980.

[21] *U.S. military handbook MIL-HDBK-1797B*, April 9, 2012.